Testing of Two-Phase Cooling of Bipolar Plates for Fuel Cells

Henk Jan van Gerner
Energy Management Group
NLR - Netherlands Aerospace Centre
Marknesse, The Netherlands
henk.jan.van.gerner@nlr.nl

Georg Mühlthaler
Environmental Control Systems
Airbus Commercial Aircraft
Hamburg, Germany
georg.muehlthaler@airbus.com

Marcus-Benedict Buntz
Research & Development Team
Aerostack GmbH
Dettingen, Germany
marcus-benedict.buntz@airbus.com

***Abstract*—Hydrogen-powered fuel cells are the preferred energy source for electric aircraft. However, for aircraft applications, it is of upmost importance to reduce the mass of the fuel cell system. A considerable amount of the total system mass is due to the fuel cell cooling system. This paper discusses two-phase cooling of the bipolar plates in a fuel cell stack. A two-step approach was used. First, test were carried out with machined plates with a geometry similar to bipolar plates. In a second step, actual bipolar plates were tested, including the membranes, seals and gaskets that are present in a fuel cell. These bipolar plates are from a standard fuel cell stack and are intended for water/glycol cooling. The tests show that these standard bipolar plates can be used with two-phase cooling with methanol.**

Keywords—two-phase, cooling, pump, fuel cell, bipolar plate

I. Introduction

In the EU funded BRAVA project, breakthrough technologies for a Fuel Cell based Power Generation System for aviation are being developed for aircraft capable of carrying up to 100 passengers on distances of up to 1,000 nautical miles. One of these technologies is the cooling system for the fuel cell stacks. A fuel cell stack contains a large number (around 500) of Membrane Electrode Assembly (MEA) with thin metal bipolar plates on both sides (Fig. 1). The coolant flows through channels between the thin metal bipolar plates, while air and H_2 flow on the opposite sides of the bipolar plates. In a previous study, a demonstrator was built for a novel two-phase pumped cooling system with 20 kW cooling capacity [1]. This system uses the evaporation of a liquid (the term "two-phase" refers to the phase transition from liquid to vapor) to remove waste heat from the heat sources, which results in a much lower mass and pump power compared to a conventional liquid cooling system [2]. However in this demonstrator, the evaporators where the waste heat is absorbed do not have a geometry representative for the bipolar plates that are used in fuel cell cooling. Fig. 2 shows a picture of a typical bipolar plate. A fuel cell stack contains gaskets and seals to separate the air, hydrogen and coolant flows. Because of the gaskets and thin bipolar plates, the coolant pressure is limited to approximately 4 barg. Methanol is used as coolant, which has an excellent thermal performance and a pressure of 3 bara at the expected operating temperature of 95°C. The coolant channel geometry is complex, since it is strongly influenced by the H_2 and air channels on the opposite sides of the bipolar plates. In order to gain more insight in cooling with bipolar plates several steps were carried out:

1. Tests with machined plates with electrical heaters. The geometry of the channels is approximately similar as for a bipolar plate.
2. Tests with bipolar plates with electrical heaters
3. Tests with a functioning fuel cell stack with two-phase cooling

The first 2 steps are discussed in this paper. The third step is currently being tested and will be discussed in a subsequent paper.

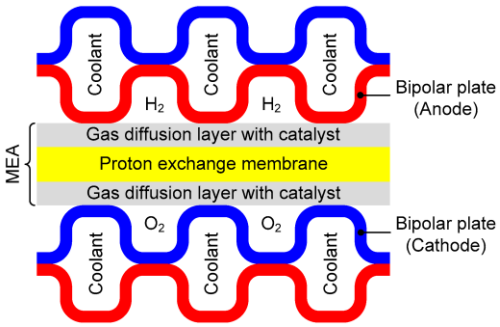

Fig. 1. Cross-section of a fuel cell stack [3].

Fig. 2. Picture of a bipolar plate assembly [4].

II. Test Setup Description

Fig. 3 shows a schematic drawing of the test setup. The pump circulates the liquid. The liquid then flows through a flowmeter. The preheater warms the liquid to the desired temperature. In the evaporator, part of the liquid is evaporated while it absorbs the heat from 10 foil heaters that are attached to the evaporator plate. Transparent flexible tubing is used to connect the evaporator inlet and outlet to the test setup. In the condenser, the vapor is condensed back into liquid. The condenser is cooled by an airflow which is generated by fans. The saturation pressure and temperature in the system (at the location of pressure sensor p_3) are controlled by the accumulator. There are 2 types of accumulators; a Heat-Controlled Accumulator (HCA) and a Pressure-Controlled Accumulator (PCA) [1]. In an HCA, both vapor and liquid are present, and the saturation temperature in the system is controlled by a heater on the vessel. In a PCA, only subcooled liquid and no vapor is present and the pressure of the liquid in the accumulator can be controlled with pressurized air or N_2 gas. This gas can be separated from the liquid by a bellows, bladder, or diaphragm, but in this setup, the N_2 gas is in direct contact with the liquid methanol. The absolute pressure is measured at four locations. The temperatures are measured at

32 locations with thermocouples while 12 separate thermocouples are used for the safety relays. There are 15 or 20 temperature sensors on the evaporator plate, see Fig. 7 and Fig. 17. The plate in the setup can be rotated in order to test it in 2 orientations (horizontal and vertical), see Fig. 4. This vertical orientation is considered to be 'worst case', since it can result in an uneven flow distribution due to gravity effects. The vertical orientation with the liquid manifold at the bottom and the two-phase manifold at the top (and vertical channels) has not been tested, since in this orientation, gravity effects result in a more even flow distribution. The plate in the setup is covered with thermal insulation. With insulation, the heat leak of the machined plate at 95°C to the ambient is measured to be 20 W. For testing with the infrared camera, the insulation is partly removed, and this increases the heat leak to 70-100 W at a plate temperature of 95°C.

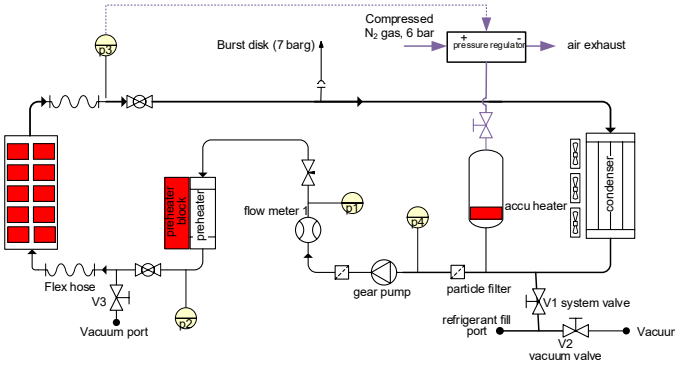

Fig. 3. Schematic drawing of the test setup.

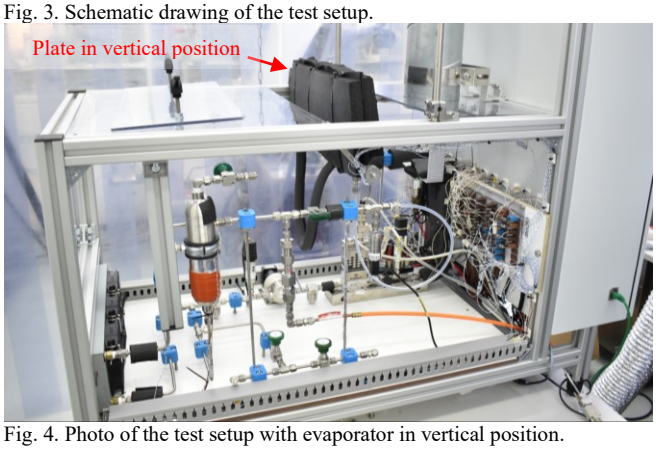

Fig. 4. Photo of the test setup with evaporator in vertical position.

III. Tests with Machined Plates with Electrical Heaters

A. Plate design

Fig. 5 shows a CAD drawing of the inlet region of the machined stainless steel (SS316) plate. The geometry of the channels approximately resembles the geometry of the coolant channels in a bipolar plate. The plate has 88 parallel square channels (in a bipolar plate, the channels are more hexagonal) with a width and height of 0.62 mm, a distance between the channels of 0.76 mm and a length of approximately 370 mm. With this channel width and height, the Eötvös (or Bond) number for methanol is 0.17, and surface tension forces dominate over gravitational forces in the channel. Note that the channels are not optimized for two-phase, e.g. channel diameter could be smaller (~25 %) for two-phase cooling. There are openings between the parallel channels (these are called 'cross-overs' and are indicated with blue in Figure 5) with a height of 0.31 mm. The flow at the inlet manifold is divided over 44 short parallel channels. The liquid is then distributed over the 88 parallel channels in the liquid distribution area, indicated with purple. The outlet region of the plate is not shown in the picture, but it is the same as the inlet region. The machined plate has a thickness of 4 mm, except near the inlet and outlet tubes, where the thickness is 8 mm. In order to improve the liquid distribution over the plate, a second variant of the plate was manufactured. This variant has flow restrictions that are located at the start of the 88 channels (indicated with yellow). These flow restrictions (which are not present in current bipolar plates) consist of very narrow passages for the liquid and have a width of 0.62 mm and a gap height of just 0.02 mm. A 1 mm thick cover plate is brazed on top of the machined plates, see Fig. 6 for a photo. This cover plate is painted black to allow for infrared measurements and 15 type T thermocouples are placed on the cover, see Fig. 7 for the locations of the temperature sensors. Ten foil heaters are glued to the back side of the plate to emulate the heat load of a fuel cell. The 10 heaters allow for different heat load distributions over the plate, although in this paper, only results with a uniform heat load are presented. The heat load per fuel cell is typically around 200 W, which results in a heat flux of 0.43 W/cm^2, which is very low compared to typical applications for two-phase cooling [5].

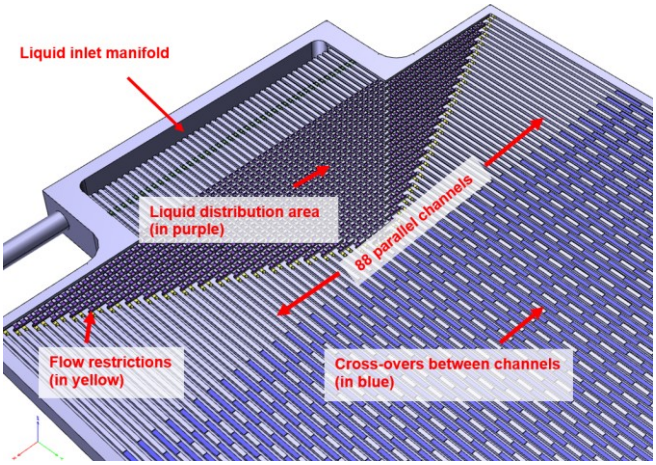

Fig. 5. Inlet region of the machined plate. The outlet region is similar.

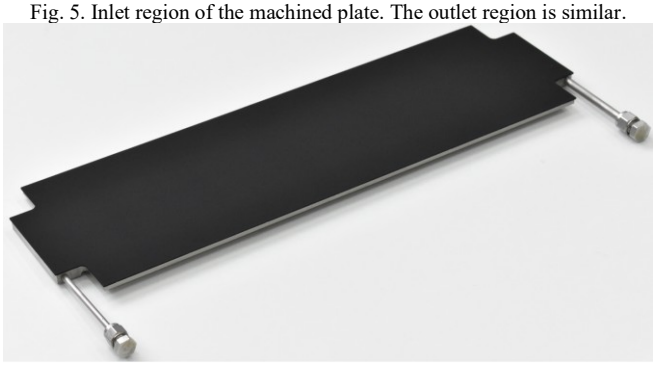

Fig. 6. Photo of the cover side.

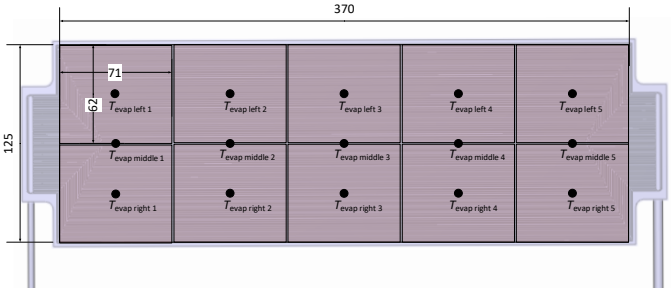

Fig. 7. Location of the temperature sensors on the cover plate side of the evaporator are indicated by the black dots. On the back side of the evaporator are 10 foil heaters (indicated with transparent-red shaded areas).

B. *Liquid distribution test*

In order to check the liquid distribution over the plates, measurements were carried out with a flow of 1.8 g/s, and an evaporator heat input of 210 W. With this heat load and mass flow, the liquid temperature remains below the setpoint saturation temperature of 95°C and the fluid remains liquid. Fig. 8 shows the measured temperatures on the second plate (with yellow flow restrictions, see Fig. 5). In steady-state, the liquid flows into the evaporator with a temperature of 28.6°C. The liquid flow out of the evaporator has a temperature of 68.1°C. This corresponds to a temperature increase of 39.5°C. The theoretical temperature of the liquid flow out of the evaporator (assuming no heat leak) is 71.6°C, which corresponds to a temperature increase of 43.0°C. The measured temperature increase is 3.5°C (or 8.1%) lower than the theoretical value, which is caused by the heat leak. The temperature on the right side of the plate is slightly higher (around 4.7°C at $T_{evap}5$) than on the left side of the plate. This can also be seen on the infrared image of the evaporator, which is shown in Fig. 9 (the insulation was partly removed for making the infrared image). This indicates that there is a small imbalance in the flow through the parallel channels of plate 2, with a higher flow (~11%) through the left channels than through the right channels. This small flow imbalance was not observed in plate 1, which is the same as plate 2, except that is does not have the small flow restrictions, i.e. it seems that the flow imbalance is caused by the flow restrictions. This might be caused by manufacturing tolerances of the very small gap height of 0.02 mm of the flow restriction. The observed flow imbalance does not have a significant influence on the two-phase cooling characteristics.

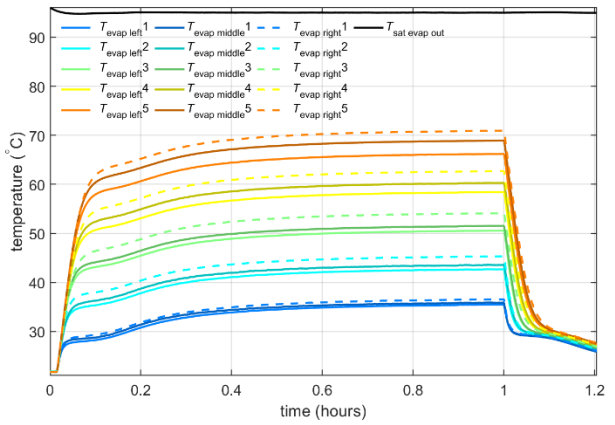

Fig. 8. Measured temperatures on the evaporator plate 2.

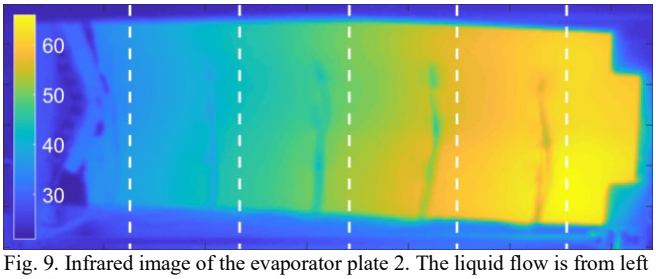

Fig. 9. Infrared image of the evaporator plate 2. The liquid flow is from left to right.

C. *Two-phase cooling with plate 1, horizontal orientation, 0.52 g/s flow*

Fig. 10 shows the measured temperatures on the machined evaporator plate 1 in horizontal position. The pump circulates a massflow of 0.52 g/s. The saturation temperature in the evaporator is set to 95°C with the accumulator. The preheater warms the liquid to a temperature of approximately 89°C before it enters the evaporator. At t=0.4 hours, a heat load of 210 W is applied on the evaporator plate. As a result, the evaporator temperature rises quickly. The liquid is superheated before it starts to evaporate and the evaporator plate reaches a peak temperature of 114°C after which the temperature of all 15 temperature sensors on the evaporator plate quickly drop to a temperature around the saturation temperature of 95°C. Methanol is very prone to liquid superheat because of the relative high surface tension and high Joule-Thomson coefficient. Also, low heat flux applications are more prone to liquid superheat. When the liquid starts to evaporate, cold liquid flows into the accumulator which causes a sudden decrease in the saturation temperature. The vapour mass fraction at the exit of the evaporator is approximately 0.4. Because of the high heat transfer coefficient and the low heat flux, the temperature difference between the fluid and the evaporator is negligible. Fig. 11 shows an infrared image of the evaporator plate. For this image, the thermal insulation was removed from one side and the heat load was 290 W to compensate for the heat leak. This infrared image also shows a uniform temperature of the evaporator plate. After post-processing of the infrared data, it was noticed that the thermocouples were not at the correct location; they should be located further downstream (see drawing Fig. 7). After the measurements with the infrared camera, the thermocouples where moved to the correct location, and all the measurements presented in this document were done with the thermocouples at the correct location.

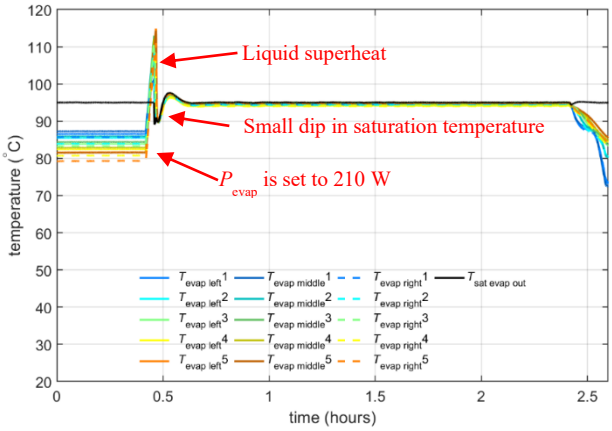

Fig. 10. Measured temperatures on the machined evaporator plate 1 in horizontal orientation with 0.52 g/s flow.

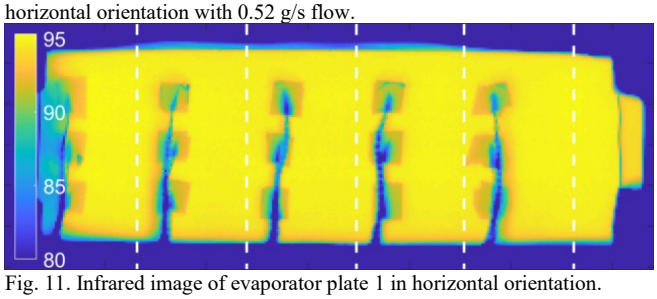

Fig. 11. Infrared image of evaporator plate 1 in horizontal orientation.

D. *Two-phase cooling with plate 1, vertical orientation, 0.52 g/s flow*

Fig. 12. shows the measured temperatures on the machined evaporator plate 1. The test conditions are the same as in the test described in the previous section, except that the plate is now in vertical orientation (see Figure 15). According

to the temperatures measured with the thermocouples, the evaporator plate has a uniform temperature in the vertical position. However, the infrared image (see Fig. 13) shows a hotspot at the top right corner. This indicates that due to gravity, there is a higher flow through the bottom channels than through the top channels and this results in dry-out and higher temperatures near the exit of the higher channels. The reason for this is that the frictional pressure drop in the channels (around 0.7 kPa according to the Müller-Steinhagen & Heck correlation [6]) is of the same order of magnitude as the pressure difference caused by gravity and the elevation difference between the bottom and top channels (0.9 kPa). There are several methods to prevent dry-out. The most simple one is to increase the mass flow, but this method is less favorable because it increases the required system pump power. Another method is to add flow restrictions at the inlet of each channel, such that the pressure difference due to the flow restriction is dominant over the pressure difference due to gravity. Both methods are discussed in the next sections. A third method is to decrease the width and height of the channels (e.g. with 25%), such that frictional pressure drop in the channels becomes dominant over the pressure difference due to gravity.

E. Two-phase cooling with plate 1, vertical orientation, 0.92 g/s flow

Fig. 14 shows the infrared image of the machined evaporator plate 2 in vertical orientation. The test conditions are the same as in the test described in the previous section, except that the mass flow is 0.92 g/s instead of 0.52 g/s. With this higher flow, no dry-out is observed. The vapour mass fraction at the exit of the evaporator is 0.2.

F. Two-phase cooling with plate 2 (with flow restrictions), vertical orientation, 0.52 g/s flow

Fig. 15 shows the infrared image of the machined evaporator plate 2 in vertical orientation. This plate is the same as plate 1, except that this plate has flow restrictions at the inlet of each channel, see Fig. 5. The test conditions are exactly the same as in section III.D, but because of the added flow restrictions, no dry-out is observed. The pressure drop over the evaporator plate is less than 0.05 bar.

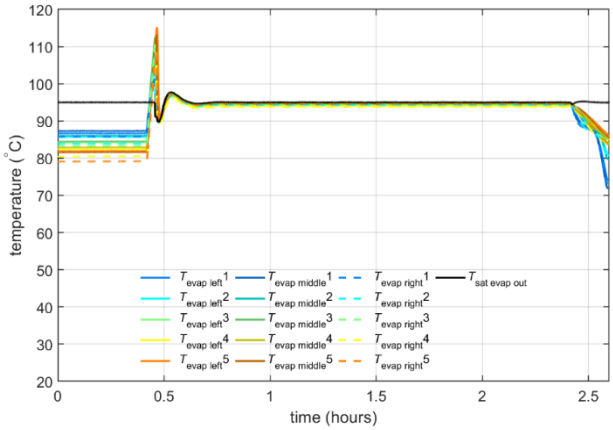

Fig. 12. Measured temperatures on the machined evaporator plate 1 in vertical orientation with 0.52 g/s flow.

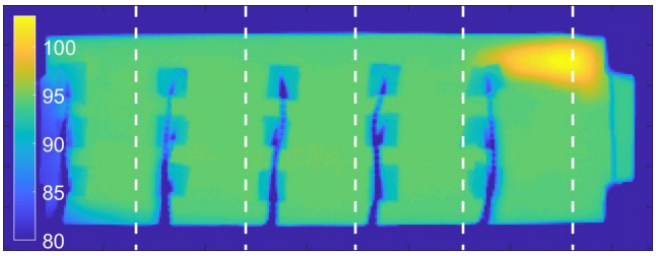

Fig. 13. Infrared image of evaporator plate 1 in vertical orientation with 0.52 g/s flow.

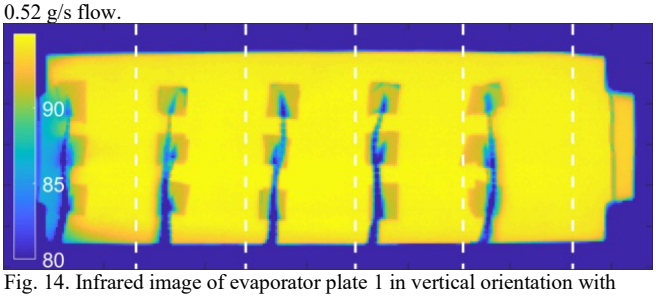

Fig. 14. Infrared image of evaporator plate 1 in vertical orientation with 0.92 g/s flow.

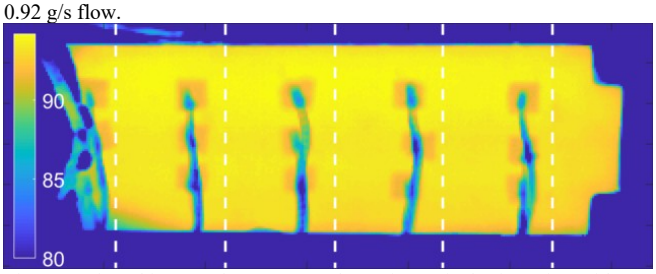

Fig. 15. Infrared image of evaporator plate 2 in vertical orientation with 0.52 g/s flow.

G. Two-phase cooling with 600 W heat load

In the previous measurements, the heat load was set to 210 W, which is the typical maximum heat load for current single fuel cells in a fuel cell stack. However, future fuel cell stacks are expected to have a higher power density and therefore higher amount of waste heat per bipolar plate. For this reason, a test was carried out in which the heat load is increased in steps from 100 W to 600 W. The mass flow is scaled with the heat load such that the vapor fraction at the exit of the evaporator is approximately 0.4. These tests show that the heat load does not have a significant influence on the temperatures and that there is a large margin to increase the power density.

H. System with PCA instead of HCA

The tests described in the previous sections were carried out with a Heat-Controlled Accumulator (HCA). For the cooling in the BRAVA system, it was decided to use a Pressure-Controlled Accumulator (PCA) [1]. For this reason, a pressure regulator was connected to the top of the accumulator vessel to control the pressure in the system with pressurized N_2 gas. A test with similar conditions as in III.C was carried out with evaporator plate 2. Fig. 16 shows the measured temperatures. Around t=1.4 hours, the saturation temperature in the setup is set to 90°C and at 1.8 hours, it is set back to 95°C. Interestingly, no liquid superheat is observed in this test. This is likely caused by the sharp edge of the flow restrictions and the presence of dissolved gas in the methanol, which is released into the liquid when the liquid nears the boiling temperature.

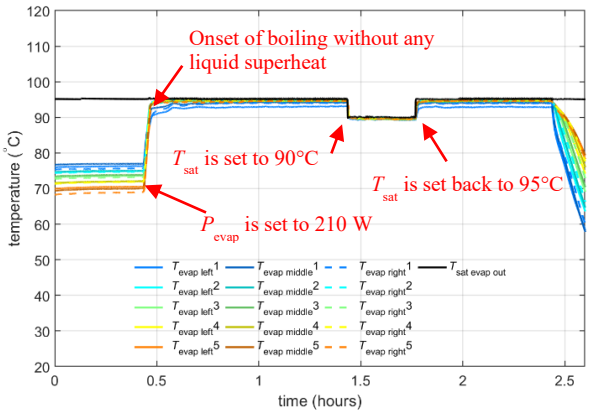

Fig. 16. Measured temperatures on the machined evaporator plate 2 with PCA.

IV. Tests with Bipolar Plates with Electrical Heaters

A. Plate design

Fig. 17 shows a CAD drawing of the thermal cell to test the bipolar plates. This thermal cell was provided by Aerostack. The bipolar plates (similar to the ones in Fig. 2) are from a standard fuel cell stack and are intended for water/glycol cooling. In the center (indicated with purple) is the bipolar plate assembly (BPA), which consists of 2 bipolar plates through which the coolant flow. Similarly as in a fuel cell stack (see Figure 5), there is a Gas Diffusion Layer (GDL, indicated with green) on both sides of the BPA. The waste heat of a fuel cell is emulated with 10 heaters on an aluminum heat distribution layer on both sides of the BPA (so 20 heaters in total). Each heat distribution layer also contains 10 type T thermocouples (of which the tip is located near the center of each heater) to measure the temperatures. The thermal cell is pressed together with endplates with a PTFE layer between the endplates and the heat distribution layers for thermal insulation. This thermal cell was then installed in the test setup as described in section II. The heat leak at 95°C to the ambient is measured to be 80 W.

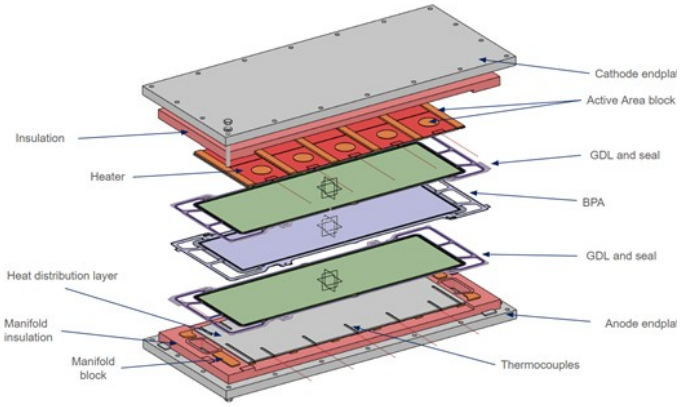

Fig. 17. CAD drawing of the bipolar plate thermal cell.

B. Liquid distribution test

In order to check the liquid distribution over the bipolar plates, a measurement was carried out with a flow of 1.8 g/s, and an evaporator heat input of 210 W (similar to the test described in III.B). Fig. 18 shows the measured temperatures on the bottom distribution layer (the figure for the top distribution layer is very similar). This test shows that the liquid is evenly distributed over the channels.

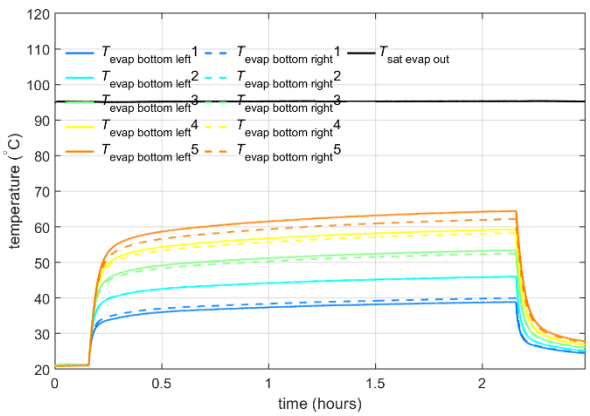

Fig. 18. Measured temperatures on the bottom heat distribution layer.

C. Two-phase cooling with bipolar plates, horizontal orientation, 0.52 g/s flow

Fig. 19 and Fig. 20 show the measured temperatures on the top and bottom heat distribution layers with the assembly in horizontal position. The pump circulates a massflow of 0.52 g/s. The saturation temperature in the evaporator is set to 95°C with the PCA. The preheater warms the liquid to a temperature of approximately 70°C before it enters the evaporator. At t=0.15 hours, a heat load of 290 W (210 W to emulate the waste heat of a fuel cell and 80 W to compensate for the heat leak) is applied. As a result, the temperature of the heat distribution layers rises quickly until the liquid starts to boil and the temperature of all 20 temperature sensors remain around 100°C, which is 5°C above the saturation temperature of 95°C. This temperature difference of 5°C is caused by the thermal resistance of the GDL and the different interfaces between the heat distribution layers and the bipolar plates. No liquid superheat is observed in this test. The vapour mass fraction at the exit of the evaporator is approximately 0.4.

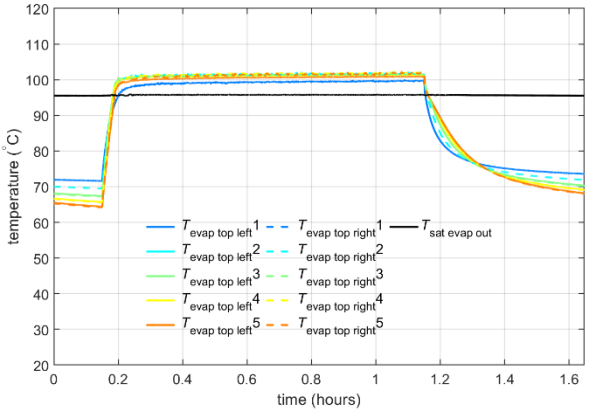

Fig. 19. Measured temperatures on the top heat distribution layer.

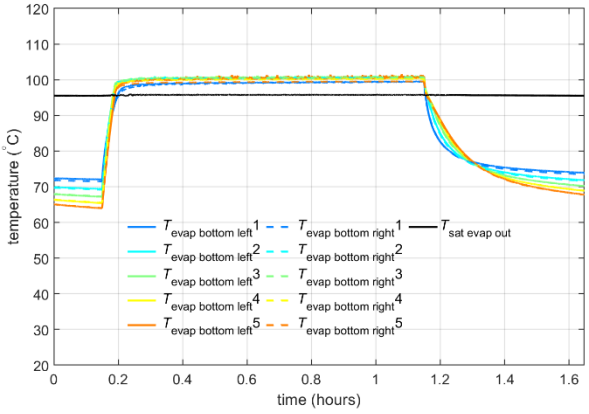

Fig. 20. Measured temperatures on the bottom heat distribution layer.

D. *Two-phase cooling with bipolar plates, vertical orientation, 0.52 g/s flow*

Fig. 21 shows the measured temperatures on the bottom heat distribution layer. The test conditions are the same as in the test described in the previous section, except that the plate is now in vertical orientation. As a result of gravity, there is a temperature difference between the left and right sides of the heat distribution layers, even near the inlet, so it seems that the channels with the highest location receive no or less liquid.

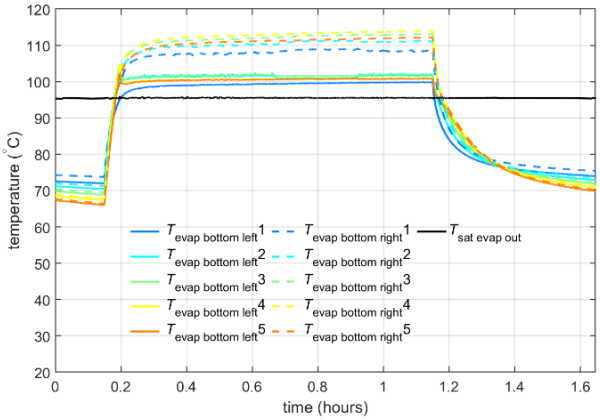

Fig. 21. Measured temperatures on the bottom heat distribution layer, 0.52 g/s, vertical orientation.

E. *Two-phase cooling with bipolar plates, vertical orientation, 0.92 g/s flow*

Fig. 22 shows the measured temperatures on the bottom heat distribution layer. The test conditions are similar as in the test described in the previous section, except that the flow is increased to 0.92 g/s (resulting in a vapor mass fraction of 0.2 at the exit of the evaporator). Despite the higher flow, there is still a significant temperature difference between the left and right sides of the heat distribution layers, even near the inlet. In order to achieve a more uniform flow distribution in vertical orientation, flow restrictions should be added, or the width and height of the channels should be decreased (e.g. with 25%), such that frictional pressure drop in the channels becomes dominant over the pressure difference due to gravity. The non-uniform flow distribution might also be caused by a 'ballooning' effect of the bipolar plates: In the setup, the bipolar plates are pressed together with endplates with a PTFE layer and a layer with foil heaters between the endplates and the bipolar plates. This intermediate layers (which are not present in an actual fuel cell) might be compressed because of the pressure inside the bipolar plates, and this could result in a gap between the bipolar plates which could result in liquid draining from the higher to the lower channels.

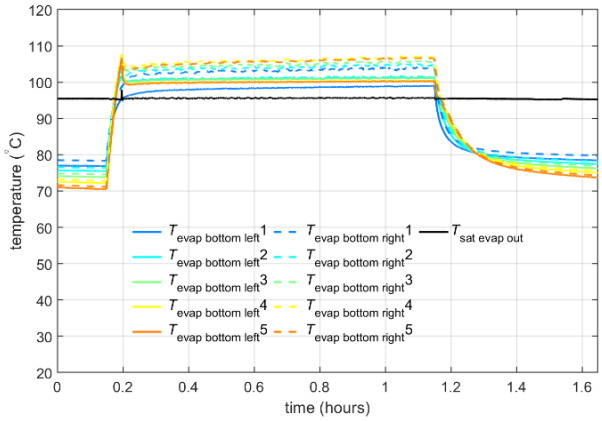

Fig. 22. Measured temperatures on the bottom heat distribution layer, 0.92 g/s, vertical orientation.

V. Conclusion and Discussion

The tests show that two-phase cooling of bipolar plates including the membranes, seals and gaskets that are present in a fuel cell, is feasible. The bipolar plates used in these tests are intended for liquid water/glycol cooling and were not optimized for two-phase cooling. Optimization of the plates would include e.g. the reduction of the channel diameter with approximately 25%. No material compatibility issues with methanol were observed during the tests. Long term material compatibility is currently further being investigated. Because of the promising results in this study, tests with two-phase cooling of a functioning fuel cell stack are currently being carried out.

Acknowledgment

This BRAVA project is funded by the European Union's Horizon Europe program under grant agreement number 101101409. This publication reflects the authors' views. Neither the European Union nor the Clean Hydrogen Joint Undertaking can be held responsible for them.

References

[1] H. van Gerner, T. Luten, S. Scholten, G. Mühlthaler and M.-B. Buntz, "Test Results for a Novel 20 kW Two-Phase Pumped Cooling System for Aerospace Applications," *Aerospace,* vol. 12, 2025.

[2] H. van Gerner, T. Luten, W. Resende, G. Mühlthaler and M.-B. Buntz, "ystem Analysis and Comparison Between a 2 MW Conventional Liquid Cooling System and a Novel Two-Phase Cooling System for Fuel Cell-Powered Aircraft.," *Energies,* 2025.

[3] D. M. Neto, M. C. Oliveira, J. L. Alves and L. F. Menezes, "Cross-section of a fuel-cell stack," *Metals,* vol. 9, no. Modelling and Simulation of Sheet Metal Forming Processes, p. 810, 2019.

[4] EKPO, "Metallic bipolar plates," [Online]. Available: https://elringklinger.de/en/products-technologies/fuel-cells/ekpo/metallic-bipolar-plates. [Accessed 28 5 2025].

[5] H. van Gerner, C. Cao, D. A. Pedroso, A. K. te Nijenhuis, I. Castro and H. Dsouza, "Two-phase pumped cooling system for power electronics; analyses and experimental results," in *30th International Workshop on Thermal Investigations of ICs and Systems (THERMINIC)*, Toulouse, 2024.

[6] H. Müller-Steinhagen and K. Heck, "A simple friction pressure drop correlation for two-phase flow in pipes," *Chemical Engineering and Processing: Process Intensification,* vol. 20, no. 6, pp. 297-308, 1986.

[7] R. Span, R. Beckmüller, S. Hielscher, A. Jäger, E. Mickoleit, T. Neumann, S. M. Pohl, B. Semrau and M. Thol, *TREND. Thermodynamic Reference and Engineering Data 5.0.,* Lehrstuhl für Thermodynamik, Ruhr-Universität Bochum, 2020.